EDGE ARTICLE

Acyclic diaminocarbene-based Thiele, Chichibabin, and Müller hydrocarbons†

Avijit Maiti, [ID] ‡[a] Shubhadeep Chandra,‡[b] Biprajit Sarkar [ID] *[b] and Anukul Jana [ID] *[a]

Thiele, Chichibabin and Müller hydrocarbons are considered as classical Kekulé diradicaloids. Herein we report the synthesis and characterization of acyclic diaminocarbene (ADC)-based Thiele, Chichibabin, and Müller hydrocarbons. The calculated singlet–triplet energy gaps are ΔE_{S-T} = −27.96, −3.70, −0.37 kcal mol^{-1}, respectively, and gradually decrease with the increasing length of the π-conjugated spacer (*p*-phenylene *vs. p,p′*-biphenylene *vs. p,p″*-terphenylene) between the two ADC-scaffolds. In agreement with the calculations, we also experimentally observed the enhancement of paramagnetic diradical character as a function of the length of the π-conjugated spacer. ADC-based Thiele's hydrocarbon is EPR silent and exhibits very well resolved NMR spectra, whereas ADC-based Müller's hydrocarbon displays EPR signals and featureless NMR spectra at room temperature. The spacer also has a strong influence on the UV-Vis-NIR spectra of these compounds. Considering that our methodology is modular, these results provide a convenient platform for the synthesis of an electronically modified new class of carbon-centered Kekulé diradicaloids.

Introduction

In recent years the chemistry of stable Kekulé diradicaloids has attracted special attention due to their unique properties and their significant importance in modern chemical physics.[1] Kekulé diradicaloids possess a characteristic resonance structure between a closed-shell quinonoid and an open-shell diradical form. In this regard, Thiele's hydrocarbon **Ia**,[2] Chichibabin's hydrocarbon **Ib**,[3] and Müller's hydrocarbon **Ic**[4] represent classical examples of Kekulé diradicaloids (Scheme 1). Kekulé diradicaloid analogues of **Ia–c** have been reported, and these range from polycyclic hydrocarbons **II**[5] to a replacement of the diphenylcarbene-scaffold (Ph$_2$C) by isoelectronic motifs such as aminium (Ar$_2$N$^+$) **III**,[6] N-heterocyclic carbene (NHC) **IV**,[7] and cyclic(alkyl)(amino)carbene (CAAC) **V** (Scheme 1).[8] The properties arising from these Kekulé diradicaloids are strikingly different from each other. Therefore, the changing of the diphenylcarbene-scaffold of **Ia–c** with isoelectronic motifs should lead to electronically tunable novel diradicaloids.[9]
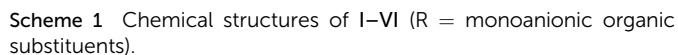
In the case of carbene chemistry it has been documented that changing of substituents at the carbenic carbon-centre leads to the electronic state alteration from triplet to singlet and *vice versa*.[10] For instance diphenylcarbene is triplet in its ground state and has been studied in matrix isolation experiments.[11] Changing the phenyl-substituent with an amino-substituent leads to an isolable singlet carbene namely acyclic diaminocarbene (ADC)[12] which has been used as a ligand in transition metal coordination chemistry[13] and in catalysis.[14] Due to the open-framework of acyclic diaminocarbenes (ADCs), the N–C(carbenic carbon)–N bond angle is wider in comparison to that of cyclic diaminocarbenes. Moreover, the conformational flexibility at the *N*-centres is much more than in cyclic diaminocarbenes. As a result the steric- as well as electronic-properties of acyclic diaminocarbene (ADC) are very much different from those of cyclic diaminocarbenes.[15] For instance ADCs are stronger σ-donors and π-acceptors compared to both cyclic imidazolidin-2-ylidenes, which are non-aromatic 5-membered NHCs with a saturated backbone, and cyclic imidazole-2-ylidenes, which are aromatic 5-membered NHCs with an unsaturated backbone.[16] Moreover, the synthetic routes for ADCs are relatively simpler than those of cyclic diaminocarbenes with a huge substrate scope.[17] Furthermore, recent results show that carbene-derived diradicaloids[18] can function as a new class of singlet fission materials.[19] We were thus interested in considering the replacement of diphenylcarbene-scaffold (Ph$_2$C) of **Ia–c** by an acyclic diaminocarbene (ADC)-motif. The envisaged compounds will represent a new class of diradicaloids with tunable spin states and electronic properties. Herein we present the synthesis and

[a]Tata Institute of Fundamental Research Hyderabad, Gopanpally, Hyderabad-500046, Telangana, India. E-mail: ajana@tifrh.res.in

[b]Universität Stuttgart, Fakultät Chemie, Lehrstuhl für Anorganische Koordinationschemie, Institut für Anorganische Chemie, Pfaffenwaldring 55, D-70569, Stuttgart, Germany. E-mail: biprajit.sarkar@iac.uni-stuttgart.de

‡ A. M. and S. C. contributed equally.

Scheme 1 Chemical structures of I–VI (R = monoanionic organic substituents).

Scheme 2 Synthesis of **3a**, **3b** and **3c**.

characterization of isolable acyclic diaminocarbene (ADC)-based Thiele, Chichibabin, and Müller hydrocarbons **VI** as Kekulé diradicaloids (Scheme 1).

Results and discussion

Keeping in mind that acyclic diaminocarbene (ADC)-based Thiele, Chichibabin, and Müller hydrocarbons possess a resonance structure of open-shell diradical form, we have considered the corresponding dications as a surrogate to gain synthetic access to these compounds.[20] Accordingly, we have chosen 1,4-dibromobenezene **1a**, 4,4′-dibromobiphenyl **1b**, and 4,4″-dibromo-p-terphenyl **1c** as readily available precursors, respectively to synthesize the targeted dications in a modular approach (Scheme 2).[21]

Three *in situ* sequential reactions of **1a**, **1b**, and **1c** with two equivalents of *n*BuLi, N,N′-diisopropylcarbodiimide, and methyl iodide lead to **2a**, **2b**, and **2c**, respectively in a good yield (Scheme 2).[21] Formation of **2a**, **2b**, and **2c** has been confirmed by ^{1}H and ^{13}C{^{1}H} NMR spectroscopy. Further the formation of **2b** and **2c** has been confirmed by the solid-state molecular structure determination (see Fig. S57 in the ESI†).[21] The subsequent reactions of **2a**, **2b**, and **2c** with two equivalents of MeOTf lead to the bis-amidinium cations **3a** (76%), **3b** (87%), and **3c** (89%),

respectively in a very good yield (Scheme 2).[21] Compounds **3a**, **3b** and **3c** have been characterized by solid-state molecular structure analysis (see Fig. S58 in the ESI†)[21] along with ^{1}H, ^{13}C{^{1}H} and ^{19}F{^{1}H} NMR spectroscopy, elemental analysis, and HRMS. Among the possible conformations, bis-amidinium dications **3a–3c** adopt a pseudo-*cis* orientation in the solid-state in which four methyl groups are in an *anti*-arrangement with respect to the π-conjugated spacer.[22] The solid state molecular structures of **3a**, **3b** and **3c** reveal the presence of C2-symmetry which also has been reflected in their solution state ^{1}H and ^{13}C{^{1}H} NMR spectra. In the ^{13}C{^{1}H} NMR spectra the most downfield shifted signals are at δ = 169.5, 170.9, and 171.2 ppm, respectively for **3a**, **3b** and **3c** which are for the ^{13}C-nuclei that are flanked between the two nitrogen centres (see Fig. S4, S14 and S23 in the ESI†).

The cyclic voltammograms of **3a–3c** were measured in $CH_3CN/0.1$ M Bu_4NPF_6 using a glassy carbon (GC) working electrode (Fig. 1).[21] A first reduction wave for **3a**, **3b** and **3c** is observed at −1.42, −1.61 and −1.82 V *vs.* FcH/FcH⁺, respectively. For all three cases the peak-to-peak separation between the forward and the reverse wave is rather small (40–50 mV), and this fact already points to the two-electron nature of the
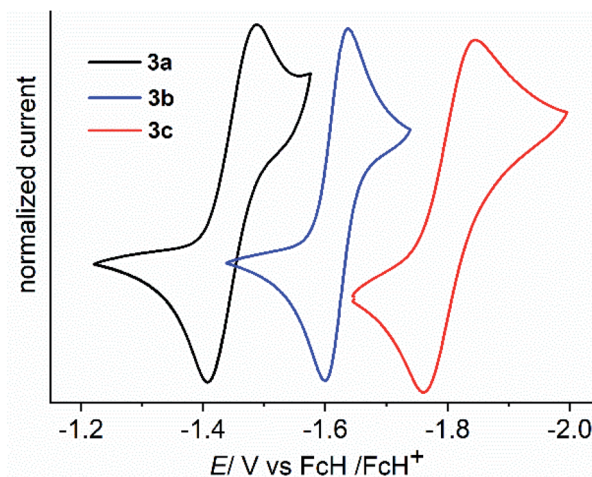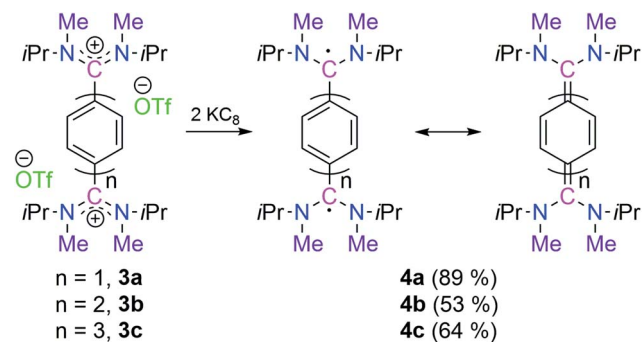

Fig. 1 Cyclic voltammograms of **3a** (black), **3b** (blue) and **3c** (red) displaying the 1st reduction in $CH_3CN/0.1$ M Bu_4NPF_6 measured at a GC working electrode with 100 mV s⁻¹.

Scheme 3 Synthesis of **4a**, **4b** and **4c**.

reduction waves. UV-Vis-NIR spectroelectrochemical measurements deliver spectra (see Fig. S44–S46 in the ESI†) after the first reduction waves that match perfectly with the spectra of the isolated two-electron reduced species (*vide infra*), thus providing further evidence for the two-electron nature of the first reduction waves.[21] This observation is similar to what we had recently reported for the dication of compound **V** (−1.36 V *vs.* FcH/FcH⁺), and shows the stability of the two-electron reduced form possibly enabled through a quinoidal structure.[8] However, the dications for NHC-based Thiele and Chichibabin hydrocarbons (**IVa–b**) exhibit two one-electron redox waves.[7a,b] The first reduction occurs at relatively lower reduction

potentials (−0.80 to −1.29 V *vs.* FcH/FcH⁺). This could be due to the relatively larger structural reorganization in the case of ADC-systems than that of NHC-systems after reduction which has been evidenced by the change of angle between the planes involving the carbene-scaffold (N1–C1(carbenic carbon)–N2) and adjacent aryl ring (C3–C2–C4′/C7) of starting dications (**3a–c**) to the corresponding two-electron reduced compounds (**4a–c**) (see Scheme 3 and Table 1). Compounds **3b** and **3c** display further irreversible reduction steps (see Fig. S42 and S43 in the ESI†), which we tentatively assign to the reduction of the extended spacers.[21]

Subsequently, the reduction of **3a**, **3b**, and **3c** with two equivalents of KC₈ led to **4a** (89%, pale yellow), **4b** (53%, dark blue), and **4c** (64%, dark green), respectively as crystalline solids (Scheme 3).[21] ¹H NMR spectrum of **4a** shows a singlet at $\delta = 6.32$ ppm for the central phenyl protons which is very much upfield shifted in comparison to **3a** ($\delta = 7.81$ ppm). In the case of **4b** two doublets appeared for the central biphenyl protons at $\delta = 7.30$ and 6.53 ppm with a coupling constant of $^3J_{(^1H,^1H)} = 9.6$ Hz.

The $^{13}C\{^1H\}$ NMR spectra of **4a** and **4b** display downfielded resonances at $\delta = 147.4$ and 150.0 ppm (see Fig. S7 and S17 in the ESI†), respectively for the ¹³C-nuclei which are flanked between the two nitrogen atoms. In the case of **4c** the ¹H NMR spectrum at room temperature displays a featureless broad signal only for the alkyl region, and there are no significant

Table 1 Selected bond lengths (Å), bond angles (°) and other selected crystallographic parameters of **3a–c**, **4a–c**, **Ia–b**, **IVa–c** and **V**

Compound	N₁–C₁	N₂–C₁	C₁–C₂	C₂–C₃	C₃–C₄	C₅–C₅′/C₈	∠N₁–C₁–N₂	∑N [°]	BLA [Å]	Angle between N1–C1–N2 and C3–C2–C4′/C7 planes
3a	1.324	1.321	1.489	1.389	1.376	—	123.279	359.9	0.02	64.818
4a	1.386	1.396	1.383	1.435	1.344	—	113.89	358.7	0.09	24.372
Ia	—	—	1.381	1.449	1.346	—	—	—	0.10	—
IVa$^{\text{IPr}a}$	1.415	1.417	1.376	1.452	1.355	—	104.577	353.9	0.09	9.171
IVa$^{\text{SIPr}b}$	1.407	1.405	1.365	1.448	1.347	—	107.878	350.9	0.10	13.263
V	1.396	—	1.381	1.452	1.352	—	—	358.1	0.10	—
3b	1.334	1.320	1.489	1.390	1.377	1.480	123.448	359.9	0.02	66.674
4b	1.382	1.396	1.387	1.437	1.347	1.407	114.11	358.5	0.09	25.079
Ib	—	—	1.415	1.424	1.372	1.448	—	—	0.05	—
IVb$^{\text{IPr}a}$	1.393	1.400	1.388	1.443	1.358	1.413	104.643	356.9	0.08	19.804
IVb$^{\text{SIPr}b}$	1.383	1.397	1.386	1.442	1.360	1.409	107.886	351.7	0.08	15.332
3c	1.335	1.323	1.494	1.384	1.380	1.491	123.126	359.9	0.00	62.550
4c	1.379	1.379	1.401	1.437	1.360	1.435	114.86	358.3	0.07	28.553
IVc$^{\text{IPr}a}$	1.399	1.400	1.401	1.439	1.364	1.431	104.529	358.65	0.07	5.433
IVc$^{\text{SIPr}b}$	1.382	1.391	1.398	1.436	1.361	1.433	107.985	349.9	0.07	19.031

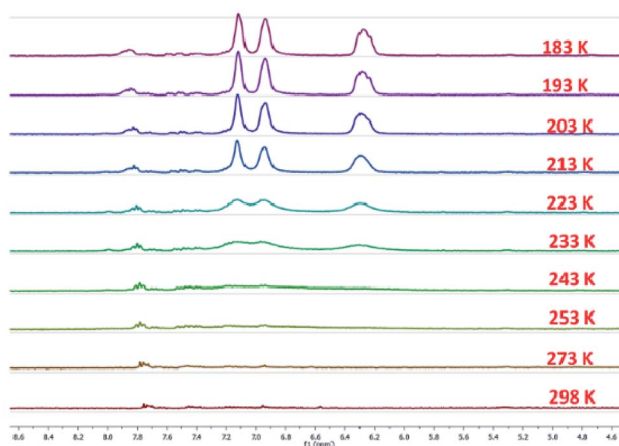^{a} IPr for imidazole-2-ylidene based NHC. ^{b} SIPr for imidazolin-2-ylidene based NHC.

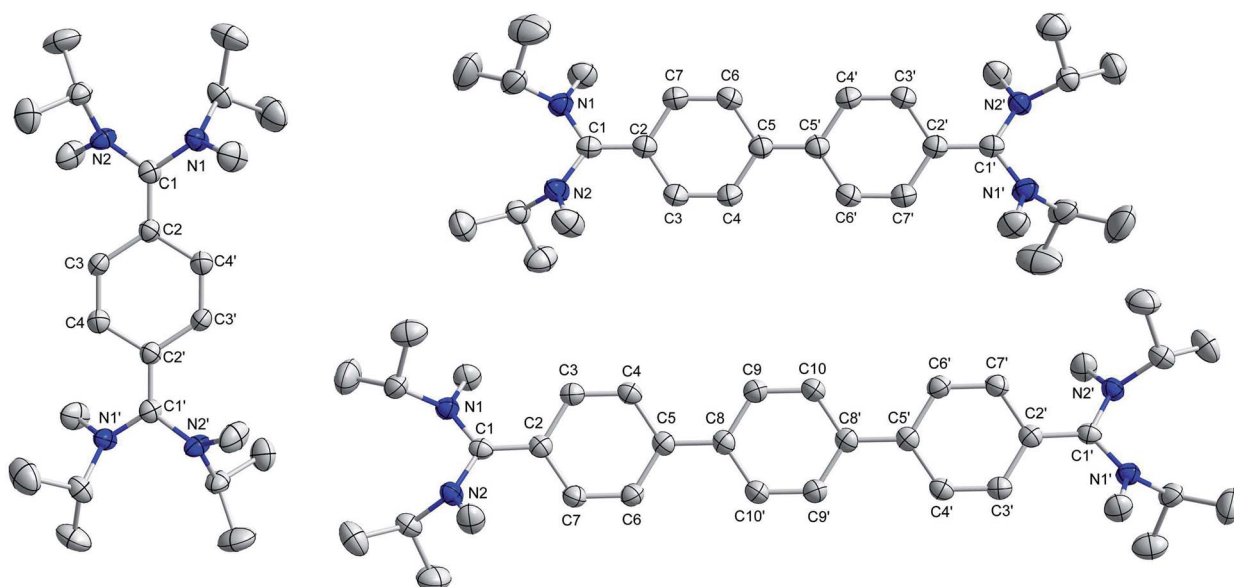Fig. 2 Selected region of the temperature-dependent ^{1}H NMR spectra of 4c in THF-d8.

signals in the aromatic region (Fig. 2). The absence of the ^{1}H NMR signals of the aromatic hydrogens at room temperature indicates a diradical contribution of 4c even at room temperature.[23] On lowering the temperature to 233 K it shows proton signals at $\delta = 7.15$, 6.96, and 6.31 ppm with equal intensity. The intensities of these signals also further increase with lowering the temperatures (Fig. 2). There was no ^{13}C{^{1}H} NMR signal for 4c even at 218 K (see Fig. S27 in the ESI†). In the case of 4b at higher temperatures the signal intensity gets reduced and peaks get broad due to a higher population of the paramagnetic triplet diradical state (see Fig. S18 in the ESI†).[21]

Compounds 4a and 4b are well soluble in benzene, toluene, and THF. This is in contrast to 4c which is soluble in THF only. Compounds 4a, 4b, and 4c are stable both in solution and in the solid state under an inert atmosphere for at least a month. 4a

and 4b are stable in solution and in the solid state even after six months under an inert atmosphere. 4a and 4b are also stable after melting at 136 °C and 118 °C, respectively which was confirmed by measuring ^{1}H NMR spectra (see Fig. S8 and S19 in the ESI†). Compound 4c starts to slowly decompose at room temperature after 5–6 days, whereas it is quite stable at −30 °C. It is stable for a month in the solid state but decomposes after melting at 118 °C. However, compounds 4a, 4b, and 4c are air-sensitive and decomposed within a minute in the solution state (see Fig. S39 and S40 in the ESI†).

The solid-state structures of 4a, 4b, and 4c (Fig. 3) suggest that the C–N bond lengths (1.38 to 1.39 Å) are longer than those in 3a, 3b, and 3c (1.32 to 1.33 Å) but shorter than those of the corresponding NHC-analogues IVa–c (Table 1).[7] The N–C–N bond angles of 4a, 4b, and 4c are 113.89 (2), 114.11(1), and 114.86(1)°, respectively. These angles are smaller than that in bis(diisopropylamino)carbene ($\angle$N–C–N = 121.0°)[24] but close to that in N,N′-ditertiarybutyl-N,N′-diphenyl acyclic diaminocarbene-coordinated AuCl ($\angle$N–C–N = 115.0°).[25] Among the possible conformations, 4a–4c adopt a pseudo-cis orientation in which all four methyl groups are in a syn-arrangement with respect to the π-conjugated spacer, which is in contrast to that of 3a–3c. In 4a the dihedral angle between the acyclic diaminocarbene-scaffold and the central phenyl ring is 24.36° and the two acyclic diaminocarbene-motifs are parallel to each other with a distance of 0.261 Å. In 4b the two phenyl rings of the biphenyl motif are coplanar and the two acyclic diaminocarbene-scaffolds are parallel to each other with a distance of 0.661 Å. The dihedral angle between the acyclic diaminocarbene-scaffold and the central biphenyl ring is 25.25°. The C5–C5′ bond length is 1.407(19) Å which is shorter in comparison with that of Ib (1.445 Å) (Table 1).[26]

In 4c the two terminal benzene rings of the p-terphenyl motif are parallel to each other with a distance of 0.597 Å, while the

Fig. 3 Solid-state structures of 4a (left), 4b (top-right), and 4c (bottom right). Hydrogen atoms are omitted for clarity.

middle benzene ring is twisted with respect to the terminal benzene rings. The dihedral angle between the middle benzene ring and the terminal benzene rings is 6.21°. The dihedral angle between the acyclic diaminocarbene-scaffold and the connected phenyl ring is 28.89°. The C5–C8 bond length is 1.435(23) Å which is longer than that of C5–C5' in **4b** (1.407(19) Å) but very similar to that of **Ib** (1.445 Å) (Table 1). The sum of the bond angles around C1 is 360°, and N1/N2 are 358.6° (**4a**), 358.8° (**4b**), and 358.1° (**4c**) indicating the planarity of the respective centres. The bond length alternation (BLA) of the aromatic π-conjugated spacer is different for **4a** (0.10 Å), **4b** (0.08 Å), and **4c** (0.06, and 0.04 for the middle phenyl ring). The BLA for **4a** is same as that for **Ia** and for **4b** is larger than that of **Ib** (0.05 Å) (Table 1).[26]

DFT calculations at the PBE0/def2-TZVP level of theory suggest a closed-shell singlet ground state for **4a–c**. The singlet triplet energy gaps for **4a**, **4b**, and **4c** are $\Delta E_{S-T} = -27.96, -3.70, -0.37$ kcal mol^{-1}, respectively.[21] This indicates that the singlet–triplet energy gap gradually decreases with the increasing length of the π-conjugated spacer (p-phenylene vs. p,p'-biphenylene vs. p,p''-terphenylene) between the two ADC-scaffolds. To further investigate the electronic structures we have also estimated the biradical character for compounds **4a–c**. Theoretical calculations at the PBE0/def2-TZVP level of theory suggest that **4a** has negligible biradical character while compounds **4b** and **4c** have a biradical character of 43% and 65% respectively.[21] Accordingly, compound **4a** is EPR silent just like **V**[8] whereas **4b** and **4c** exhibit EPR signals both in the solid and solution states at 298 K with a g-value of 2.004 (Fig. 4 and see Fig. S47 in the ESI†).

This fact indicates that even though the singlet state is the ground state for **4b** ($\Delta E_{S-T} = -3.70$ kcal mol^{-1}) and **4c** ($\Delta E_{S-T} = -0.37$ kcal mol^{-1}), due to the small singlet–triplet gap, the triplet state is populated to a certain extent at room temperature. Similar observations were made in related systems that were investigated recently.[7c,9a,27] This is not the case for **4a** which has a relatively larger singlet triplet gap ($\Delta E_{S-T} = -27.96$ kcal mol^{-1}).[21] Gratifyingly, the results from the EPR experiments fit nicely with the observations from the NMR experiments (vide supra). Additionally, fitting of the variable temperature EPR data with the Bleaney–Bower equation furnished further information about the singlet–triplet gaps of $\Delta E_{S-T} = -2.3$ kcal mol^{-1} for **4b** and $\Delta E_{S-T} = -0.65$ kcal mol^{-1} for **4c** which also indicate significant population of the triplet state at room temperature (see Fig. S48 and S49 in the ESI†).[21] The obtained singlet–triplet energy gaps from the solid-state variable temperature EPR study for **4b** and **4c** are very close to those of theoretically calculated values.[21]

The above observations indicate that the enhancement of paramagnetic triplet diradical character occurs with increasing the length of the π-conjugated spacer. Further support for this hypothesis comes from the bond lengths between the carbenic carbon-C1 and the attached carbon-C2 of the π-conjugated spacer (for **4a**: 1.3827(38) Å, **4b**: 1.3871(19), and **4c**: 1.4009(22) Å) (Table 1). Spin density calculations of **4a–4c** suggest that considerable unpaired electron density is located at the carboncentre which is flanked between two N-centres (Fig. 4 and see Fig. S50 in the ESI†).[21]

The UV/Vis spectra of compounds **4a**, **4b**, and **4c** exhibit their main absorption bands at $\lambda_{max} = 436$ ($\varepsilon = 77\,185$ L mol^{-1} cm^{-1}), 591 ($\varepsilon = 46\,656$ L mol^{-1} cm^{-1}), and 688 ($\varepsilon = 44\,680$ L mol^{-1} cm^{-1}) nm, respectively (Fig. 5). TD-DFT calculations suggest these to be HOMO–LUMO transitions (see Fig. S51, S53 and S55 and Tables S3, S6, and S9 in the ESI†).[21] This clearly shows that upon increasing the length of the aromatic π-conjugated spacer between the two acyclic diaminocarbenescaffolds the HOMO–LUMO gap decreases.

Remarkably, compound **4c** displays additional absorption at $\lambda_{max} = 879$ nm ($\varepsilon = 10\,572$ L mol^{-1} cm^{-1}) (Fig. 5). TD-DFT calculations on the triplet state of all three molecules suggest long wavelength bands. We hypothesize that the observance of a long wavelength band for **4c** which also absorbs in the NIR region is related to the population of the triplet state for this molecule. These UV-Vis-NIR spectra match well with those obtained from the corresponding UV-Vis-NIR spectroelectrochemical measurements (see Fig. S44–S46 in the ESI†).[21]
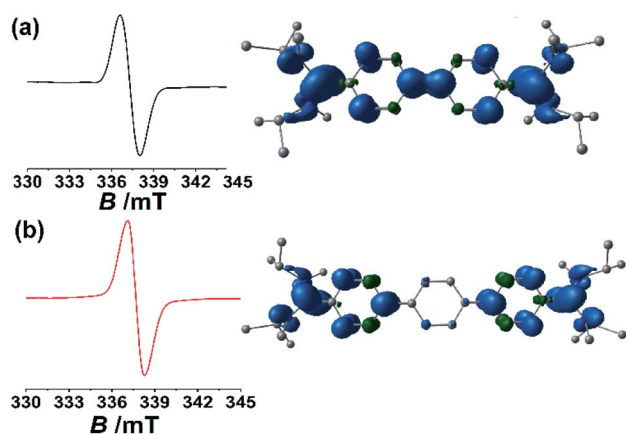

Fig. 4 Solid state EPR spectra measured at room temperature and the calculated spin density plot (with an isovalue of 0.004) at the PBE0/def2-TZVP level of theory for **4b** (a) and **4c** (b).
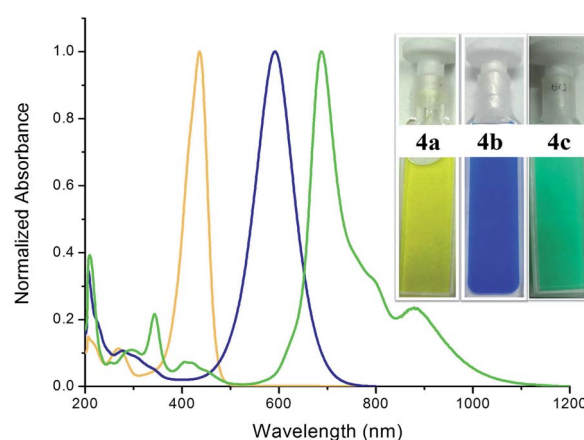

Fig. 5 Comparison of the UV/Vis spectra of **4a**, **4b**, and **4c** in THF at room temperature.

Thus, the absorption maxima of these species can be tuned over a range of greater than 250 nm. Intriguingly, **4c**, which displays the highest diradicaloid character displays absorptions that go deep into the NIR region.

Conclusions

In conclusion, we have designed and synthesized the first stable acyclic diaminocarbene (ADC)-based Thiele, Chichibabin, and Müller hydrocarbons in a modular approach. The ADC-analogues of the Chichibabin, and Müller hydrocarbons display population of the triplet state at room temperature, whereas the ADC-analogue of the Thiele hydrocarbon exhibits diamagnetic character. The straightforward synthetic methodology revealed in this study, and the resulting tuning of the spin states and the color of these compounds will be instrumental for the generation of new classes of carbon centre based Kekulé diradicaloids and polyradicaloids.[28]

Conflicts of interest

There are no conflicts to declare.

Acknowledgements

Notes and references

1 Selected references are: (*a*) T. Stuyver, B. Chen, T. Zeng, P. Geerlings, F. D. Proft and R. Hoffmann, *Chem. Rev.*, 2019, **119**, 11291–11351; (*b*) M. Abe, Diradicals, *Chem. Rev.*, 2013, **113**, 7011–7088; (*c*) K. Yang, X. Zhang, A. Harbuzaru, L. Wang, Y. Wang, C. Koh, Y. Guo, Y. Shi, J. Chen, H. Sun, K. Feng, M. C. R. Delgado, H. Y. Woo, R. P. Ortiz and X. Guo, *J. Am. Chem. Soc.*, 2020, **142**, 4329–4340; (*d*) G. E. Rudebusch, J. L. Zafra, K. Jorner, K. Fukuda, J. L. Marshall, I. Arrechea-Marcos, G. L. Espejo, R. P. Ortiz, C. J. Gómez-García, L. N. Zakharov, M. Nakano, H. Ottosson, J. Casado and M. M. Haley, *Nat. Chem.*, 2016, **8**, 753–759; (*e*) K. Kamada, S.-i. Fuku-en, S. Minamide, K. Ohta, R. Kishi, M. Nakano, H. Matsuzaki, H. Okamota, H. Higashikawa, K. Inoue, S. Kojima and Y. Yamamoto, *J. Am. Chem. Soc.*, 2013, **135**, 232–241; (*f*) C. Zhang, S. M. Rivero, W. Liu, D. Casanova, X. Zhu and J. Casado, *Angew. Chem., Int. Ed.*, 2019, **58**, 11291–11295; (*g*) J. L. Zafra, L. Qiu, N. Yanai, T. Mori, M. Nakano, M. P. Alvarez, J. T. L. Navarrete, C. J. Gómez-García, M. Kertesz, K. Takimiya and J. Casado, *Angew. Chem., Int. Ed.*, 2016, **55**, 14563–14568; (*h*) S. Dong, T. Y. Gopalakrishna, Y. Han, H. Phan, T. Tao, Y. Ni, G. Liu and C. Chi, *J. Am. Chem. Soc.*, 2019, **141**, 62–66; (*i*) G. E. Rudebusch, G. L. Espejo, J. L. Zafra, M. P. Alvarez, S. N. Spisak, K. Fukuda, Z. Wei, M. Nakano, M. A. Petrukhina, J. Casado and M. M. Haley, *J. Am. Chem. Soc.*, 2016, **138**, 12648–12654; (*j*) X. Zhu, H. Tsuji, K. Nakabayashi, S. Ohkoshi and E. Nakamura, *J. Am. Chem. Soc.*, 2011, **133**, 16342–16345; (*k*) X. Hu, W. Wang, D. Wang and Y. Zheng, *J. Mater. Chem. C*, 2018, **6**, 11232–11242.

2 J. Thiele and H. Balhorn, *Ber. Dtsch. Chem. Ges.*, 1904, **37**, 1463–1470.

3 A. E. Tschitschibabin, *Ber. Dtsch. Chem. Ges.*, 1907, **40**, 1810–1819.

4 E. Müller and H. Pfanz, *Ber. Dtsch. Chem. Ges. B*, 1941, **74**, 1051–1074.

5 (*a*) W. Zeng, T. Y. Gopalakrishna, H. Phan, T. Tanaka, T. S. Herng, J. Ding, A. Osuka and J. Wu, *J. Am. Chem. Soc.*, 2018, **140**, 14054–14058; (*b*) T. Y. Gopalakrishna, W. Zeng, X. Lu and J. Wu, *Chem. Commun.*, 2018, **54**, 2186–2199.

6 (*a*) Y. Su, X. Wang, Y. Li, Y. Song, Y. Sui and X. Wang, *Angew. Chem., Int. Ed.*, 2015, **54**, 1634–1637; (*b*) G. Tan and X. Wang, *Acc. Chem. Res.*, 2017, **50**, 1997–2006.

7 (*a*) D. Rottschäfer, N. K. T. Ho, B. Neumann, H.-G. Stammler, M. von. Gastel, D. M. Andrada and R. S. Ghadwal, *Angew. Chem., Int. Ed.*, 2018, **57**, 5838–5842; (*b*) D. Rottschafer, B. Neumann, H.-G. Stammler, D. M. Andrada and R. S. Ghadwal, *Chem. Sci.*, 2018, **9**, 4970–4976; (*c*) D. Rottschäfer, J. Busch, B. Neumann, H.-G. Stammler, M. von. Gastel, R. Kishi, M. Nakano and R. S. Ghadwal, *Chem.–Eur. J.*, 2018, **24**, 16537–16542.

8 A. Maiti, J. Stubbe, N. I. Neuman, P. Kalita, P. Duari, C. Schulzke, V. Chandrasekhar, B. Sarkar and A. Jana, *Angew. Chem., Int. Ed.*, 2020, **59**, 6729–6734.

9 (*a*) J. Wang, X. Xu, H. Phan, T. S. Herng, T. Y. Gopalakrishna, G. Li, J. Ding and J. Wu, *Angew. Chem., Int. Ed.*, 2017, **56**, 14154–14158; (*b*) M. A. Majewski, P. J. Chmielewski, A. Chien, Y. Hong, T. Lis, M. Witwicki, D. Kim, P. M. Zimmerman and M. Stępień, *Chem. Sci.*, 2019, **10**, 3413–3420.

10 (*a*) D. Bourissou, O. Guerret, F. P. Gabbaï and G. Bertrand, *Chem. Rev.*, 2000, **100**, 39–92; (*b*) K. Hirai, T. Itoh and H. Tomioka, *Chem. Rev.*, 2009, **109**, 3275–3332.

11 M. S. Platz, V. P. Senthilnathan, B. B. Wright and C. W. McCurdy Jr, *J. Am. Chem. Soc.*, 1982, **104**, 6494–6501.

12 (*a*) R. W. Alder, M. E. Blake, L. Chaker, J. N. Harvey, F. Paolini and J. Schütz, *Angew. Chem., Int. Ed.*, 2004, **43**, 5896–5911; (*b*) J. Vignolle, X. Cattoën and D. Bourissou, *Chem. Rev.*, 2009, **109**, 3333–3384; (*c*) T. Schulz, D. Weismann, L. Wallbaum, R. Guthardt, C. Thie, M. Leibold, C. Bruhn and U. Siemeling, *Chem.–Eur. J.*, 2015, **21**, 14107–14121.

13 (*a*) V. P. Boyarskiya, K. V. Luzyanina and V. Y. Kukushkin, *Coord. Chem. Rev.*, 2012, **256**, 2029–2056; (*b*)

M. A. Kinzhalov and K. V. Luzyanin, *Coord. Chem. Rev.*, 2019, **399**, 213014.

14 (*a*) B. Dhudshia and A. N. Thadani, *Chem. Commun.*, 2006, 668–670; (*b*) L. M. Slaughter, *ACS Catal.*, 2012, **2**, 1802–1816.

15 D. Martin, Y. Canac, V. Lavallo and G. Bertrand, *J. Am. Chem. Soc.*, 2014, **136**, 5023–5030.

16 K. Denk, P. Sirsch and W. A. Herrmann, *J. Organomet. Chem.*, 2002, **649**, 219–224.

17 R. W. Alder, M. E. Blake, S. Bufali, C. P. Butts, A. G. Orpen, J. Schütz and S. J. Williams, *J. Chem. Soc., Perkin Trans. 1*, 2001, 1586–1593.

18 (*a*) B. M. Barry, R. G. Soper, J. Hurmalainen, A. Mansikkamäki, K. N. Robertson, W. L. McClennan, A. J. Veinot, T. L. Roemmele, U. Werner-Zwanziger, R. T. Boeré, H. M. Tuononen, J. A. C. Clyburne and J. D. Masuda, *Angew. Chem., Int. Ed.*, 2018, **57**, 749–754; (*b*) M. M. Hansmann, M. Melaimi, D. Munz and G. Bertrand, *J. Am. Chem. Soc.*, 2018, **140**, 2546–2554.

19 (*a*) J. Messelberger, A. Grünwald, P. Pinter, M. M. Hansmann and D. Munz, *Chem. Sci.*, 2018, **9**, 6107–6117; (*b*) A. Japahuge, S. Lee, C. H. Choi and T. Zeng, *J. Chem. Phys.*, 2019, **150**, 234306; (*c*) T. Ullrich, P. Pinter, J. Messelberger, P. Haines, R. Kaur, M. M. Hansmann, D. Munz and D. M. Guldi, *Angew. Chem., Int. Ed.*, 2020, **59**, 7906–7914.

20 (*a*) D. Mandal, S. Sobottka, R. Dolai, A. Maiti, D. Dhara, P. Kalita, R. S. Narayanan, V. Chandrasekhar, B. Sarkar and A. Jana, *Chem. Sci.*, 2019, **10**, 4077–4081; (*b*) M. K. Nayak, J. Stubbe, N. I. Neuman, R. S. Narayanan, S. Maji, C. Schulzke, V. Chandrasekhar, B. Sarkar and A. Jana, *Chem.–Eur. J.*, 2020, **26**, 4425–4431.

21 See the ESI† for the experimental details, analytical data, NMR spectra, UV/Vis spectra, X-ray crystallographic details and details of theoretical calculations.

22 (*a*) E. L. Rosen, M. D. Sanderson, S. Saravanakumar and C. W. Bielawski, *Organometallics*, 2007, **26**, 5774–5777; (*b*) M. S. Collins, E. L. Rosen, V. M. Lynch and C. W. Bielawski, *Organometallics*, 2010, **29**, 3047–3053.

23 (*a*) M. M. Hansmann, M. Melaimi, D. Munz and G. Bertrand, *J. Am. Chem. Soc.*, 2018, **140**, 2546–2554; (*b*) K. Kamada, S. Fuku-en, S. Minamide, K. Ohta, R. Kishi, M. Nakano, H. Matsuzaki, H. Okamoto, H. Higashikawa, K. Inoue, S. Kojima and Y. Yamamoto, *J. Am. Chem. Soc.*, 2013, **135**, 232–241; (*c*) Y. Su, X. Wang, X. Zheng, Z. Zhang, Y. Song, Y. Sui, Y. Li and X. Wang, *Angew. Chem., Int. Ed.*, 2014, **53**, 2857–2861; (*d*) G. E. Rudebusch, J. L. Zafra, K. Jorner, K. Fukuda, J. L. Marshall, I. Arrechea-Marcos, G. L. Espejo, R. P. Ortiz, C. J. Gómez-García, L. N. Zakharov, M. Nakano, H. Ottosson, J. Casado and M. M. Haley, *Nat. Chem.*, 2016, **8**, 753–759.

24 R. W. Alder, P. R. Allen, M. Murray and A. G. Orpen, *Angew. Chem., Int. Ed. Engl.*, 1996, **35**, 1121–1123.

25 H. Seo, B. P. Roberts, K. A. Abboud, K. M. Merz Jr and S. Hong, *Org. Lett.*, 2010, **12**, 4860–4863.

26 L. K. Montgomery, J. C. Huffman, E. A. Jurczak and M. P. Grendze, *J. Am. Chem. Soc.*, 1986, **108**, 6004–6011.

27 (*a*) C. Saalfrank, F. Fantuzzi, T. Kupfer, B. Ritschel, K. Hammond, I. Krummenacher, R. Bertermann, R. Wirthensohn, M. Finze, P. Schmid, V. Engel, B. Engels and H. Braunschweig, *Angew. Chem., Int. Ed.*, DOI: 10.1002/anie.202008206; (*b*) C. H. E. Chow, Y. Han, H. Phan and J. Wu, *Chem. Commun.*, 2019, **55**, 9100–9103.

28 I. Ratera and J. Veciana, *Chem. Soc. Rev.*, 2012, **41**, 303–349.